Surface microstructure and cell compatibility of calcium silicate and calcium phosphate composite coatings on Mg–Zn–Mn–Ca alloys for biomedical application

Hui Du[a], Zunjie Wei[a,*], Hongwei Wang[a], Erlin Zhang[b], Lin Zuo[c], Lianping Du[d]

[a] School of Materials Science and Engineering, Harbin Institute of Technology, Harbin 150001, China
[b] School of Materials and Engineering, Jiamusi University, Jiamusi 154007, China
[c] China Medical University, Shenyang 110001, China
[d] Weigao Group, Weihai 264209, China

ABSTRACT

A calcium silicate and calcium phosphate ($CaSiO_3/CaHPO_4 \cdot 2H_2O$) composite coating was applied by a chemical reaction to Mg–Zn–Mn–Ca alloy to improve its biocompatiblity. The surface microstructure was observed by scanning electronic microscopy (SEM) and the surface bioactivity was assessed by a cell interaction experiment. SEM observation showed that a microporous layer was formed on the surface of Mg–Zn–Mn–Ca alloy. It was shown by XRD that the reaction layer was mainly composed of $CaHPO_4 \cdot 2H_2O$ and a small amount of $CaSiO_3$. *In vitro* cell experiments indicated that *osteoblasts* showed good adhesion, high growth rates and proliferation characteristics on the coated Mg–Zn–Mn–Ca alloy, indicating that the surface cytocompatibility of Mg–Zn–Mn–Ca alloy was significantly improved by the calcium phosphate coating.

© 2010 Elsevier B.V. All rights reserved.

1. Introduction

Mg alloys have shown potential application as bone substitute materials due to their good biocompatibility [1] and biodegradability [2–5]. The Mg ion is the fourth most prevalent constituent of human serum [6]. The mechanical properties of Mg alloys are more similar to those of human bone among the commonly used artificial implant materials [7]. However, the rapid corrosion of Mg and its alloys in human body fluid or blood plasma limits their clinical applications [8]. Therefore, improving the corrosion resistance of Mg alloys for biomedical application is very necessary. Surface treatment techniques have been successfully applied to improve their anti-corrosion properties [9]. However, for biomedical application, the surface coating should have good biocompatibility, as well as good anti-corrosion properties against surrounding bioenvironment. Calcium phosphate (Ca–P) coatings have been widely used on bone implant materials due to their favorable biocompatibility and osteoconductive properties [9–11]. The brushite ($CaHPO_4 \cdot 2H_2O$) coating is reported to improve significantly the biocorrosion resistance and osseous integration of the Mg alloy [12]. However, Ca–P ceramics show slow bone formation *in vivo* [13].

Previous research suggested that silicon, an essential element in animal nutrition, is localized in the active areas of young bone and an important role in bone metabolism [14,15]. Furthermore, $CaSiO_3$ ceramic exhibited good osteoconductivity [16], bioactivity, degradability, and biocompatibility [17,18]. Some studies have shown that $CaSiO_3$ ceramic promotes the proliferation and differentiation of osteoblast-like cells compared with Ca–P ceramics [19]. Moreover, $CaSiO_3$ can accelerate the formation of hydroxyapatite (HA) in a simulated body fluid [20]. However, $CaSiO_3$ rapidly degrades *in vitro* and *in vivo* [20], which limits its application as a bone substitute. Therefore, to improve the anti-corrosion property and cell compatibility, a $CaSiO_3$ and $CaHPO_4$ composite ($CaSiO_3/CaHPO_4 \cdot 2H_2O$) coating is proposed for use in biomedical applications.

In this study, calcium silicate and calcium phosphate composites ($CaSiO_3/CaHPO_4 \cdot 2H_2O$) were chemical coated onto Mg–Zn–Mn–Ca alloys. Moreover, the *osteoblasts* adhesion and proliferation on the $CaSiO_3/CaHPO_4 \cdot 2H_2O$ composite-coated Mg–Zn–Mn–Ca alloys are preliminarily assessed quantitatively to evaluate its bioactivity.

2. Experimental

2.1. Preparation of the $CaSiO_3/CaHPO_4 \cdot 2H_2O$ composite coating

Samples measuring $10\,mm \times 10\,mm \times 2\,mm$ were cut from an extruded Mg–Zn–Mn–Ca alloy bar prepared in our laboratory. The

Table 1
Chemical composition of the reaction bath.

Composition	Concentration, g/l
$NaSiO_3$	30
$Ca(NO_3)_2$	30

samples were ground and polished with SiC abrasive paper up to 2000 grits. The samples were initially immersed in an alkaline solution at 63 °C for 15 min for degreasing, then in 85% H_3PO_4 solution at room temperature for 20 s, and then in an activation solution (NH_4F) for 5 min. Then, the samples were treated in a reaction bath at 45 °C for 50 min. The ingredients of the reaction bath are listed in Table 1. The pH of the bath was adjusted with H_3PO_4 or H_2SO_4 to around 4.6–5.0.

2.2. Surface characterization

The surface microstructure and the morphology were observed using a Hitachi S-4700 scanning electronic microscope (SEM) coupled with energy dispersive spectroscope (EDS). The acceleration voltage used for the SEM was 15.0 kV. To identify the surface phase, the surface was examined under X-ray diffraction (XRD, D/MAX-RB, Rigaku). The 2θ range was 20–90, and the scan step size was 0.04 in XRD.

2.3. Electrochemical measurement

The electrochemical polarization tests were carried out in Hank's solution by a PARSTAT 2273 automatic laboratory corrosion measurement system. A three-electrode cell was used. The counter electrode was made of platinum and the reference electrode was saturated calomel electrode. All the measurements were carried out at a scanning rate of 0.5 mV/s at 37 °C.

2.4. Cytocompatibility test

2.4.1. Cell culture
Osteoblasts were isolated from the calvaria of neonatal (less than 24-h old) Sprague–Dawley rats (obtained from the China Medical University) through an enzymatic digestion. The rat calvaria were washed three times in phosphate-buffered saline (PBS, pH = 7.4) and then minced into 1 mm diameter fragments. After washing the bone fragments thrice with PBS, the calvaria chips were digested for 20 min, at 37 °C with 0.25% (w/v) trypsin–EDTA solution (Gibco) to diminish fibroblastic contamination. Then, the samples were treated with 0.125% I-collagenase (Sigma) at 37 °C for 90 min to release osteoblast from the calvaria. The supernates were centrifugated at 1000 rpm for 10 min, and then suspended in Dulbecco's modified Eagle's essential *medium* (DMEM) (Gibco, USA) containing 10% (v/v) heat-inactivated fetal calf serum with 50 μg/mL L-ascorbic acid, 1% glutamine, 50 U/mL penicillin/streptomycin, and incubated in a 75 cm² flask at 37 °C under a humidified 5% CO_2 atmosphere consisting. The culture media was refreshed every 2 days. The cells used in our study were between their third and fourth passages.

2.5. MTT test

MTT (3-(4,5-dimethylthiazol-2-yl)-2,5-diphenyltetrazolium bromide) colorimetric assays were used to determine toxicity against *osteoblasts*. MTT tests were carried out by indirect contact. An extraction medium was prepared according to ISO 10993-5 [21]. The bare Mg–Zn–Mn–Ca samples and the $CaSiO_3/CaHPO_4 \cdot 2H_2O$ composite-coated Mg–Zn–Mn–Ca samples were immersed in DMEM medium with serum at 37 ± 1 °C for 24 h to gain the

extraction. The control groups involve the use of DMEM medium as negative control. The ratio of the surface area of the sample to the volume of the medium was 0.5 cm²/mL. The MTT solution was prepared in PBS at a final concentration of 5 mg/mL. The *osteoblasts* were seeded in 96-well culture plates at a density of 1×10^4 cells/100 μL in each well and incubated at 37 °C in humidified a 5% CO_2 atmosphere for 24 h to allow attachment. Then, the DMEM medium was replaced by 100 μL of extracts. The plates were incubated at 37 °C for 12, 24, 48, and 96 h. At the end of each incubation time, the media were discarded and replaced with 20 μL MTT solution, and incubated for 6 h. Afterwards, the medium was discarded, and replaced with 150 μL dimethylsulfoxide. After gently shaking for 10 min, the optical density (OD) was determined with an ELISA reader at 500 nm. The cell viabilities were expressed as Relative Growth Rates (RGR) as determined by RGR (%) = (OD sample/OD negative control) × 100%. The values of the MTT were calculated based on means ± standard deviations from five wells (SD, $n = 5$). One-way ANOVA followed by a Mann–Whitney test was carried out using SPSS software. The differences between groups were considered statistically significant at $p < 0.05$. Meanwhile, the pH of the extraction medium was monitored by PHS-3C pH meter (Lei-ci, Shanghai).

2.6. Cell adhesion

The osteoblasts were seeded onto the bare Mg–Zn–Mn–Ca samples and the $CaSiO_3/CaHPO_4 \cdot 2H_2O$-coated Mg–Zn–Mn–Ca samples at a cell density of 1×10^5 cell/mL. Cultures were incubated in 24 well plates (Corning, NY, USA) at 37 °C in a humidified incubator with 5% CO_2 in air for 6, 12, and 24 h, respectively. Then, the samples were washed thrice with PBS to remove non-adherent cells, and then fixed for 24 h in 2.5% (w/v) glutaraldehyde, gradually dehydrated in 50–100 vol% alcohol. The samples were sputter-coated with gold and examined under a Hitachi S-4700 SEM. Three parallel samples were used for each experimental condition.

2.7. Determination of cell cycle stage

The distribution of cells at specific cell cycle stages was evaluated by flow cytometry. *Osteoblasts* were dispensed into 6-well culture plates at 1×10^6 cells per well and incubated in composite-coated DMEM and normal DMEM, respectively, for 12, 24, 48, and 72 h. The cells were trypsinized after washing with PBS and fixed overnight in 70% ethanol at −20 °C. After centrifugation at 800 rpm for 7 min, the cells were resuspended in 500 μL PI (0.05‰ PI, 0.02% RNase, 0.01M Triton X-100) and incubated in the dark for 30 min at room temperature. Cell cycle staging and distribution were analyzed by flow cytometry (BD FACS Calibur, USA) and the data were analyzed by Mann–Whitney test, which was carried out by SPSS software. All data were calculated based on the average of triplicate (SD, $n = 3$).

3. Result

3.1. Phase identification and Microstructure

SEM micrographs show that the Mg–Zn–Mn–Ca samples were completely covered by a gray film after 50 min conversion treatment. Under low magnification, as shown in Fig. 1a, large numbers of cracks are found on the surface due to dehydration shrinkage. Under high magnification, as shown in Fig. 1b, a porous structure is clearly observed. EDS analysis conducted on the coating, as shown in Fig. 1c, indicates that the surface is mainly composed of O, P, Si, Ca, and Mg, and the Si content is 4.22 wt.%. XRD was conducted on the coating to identify its phase constitution,
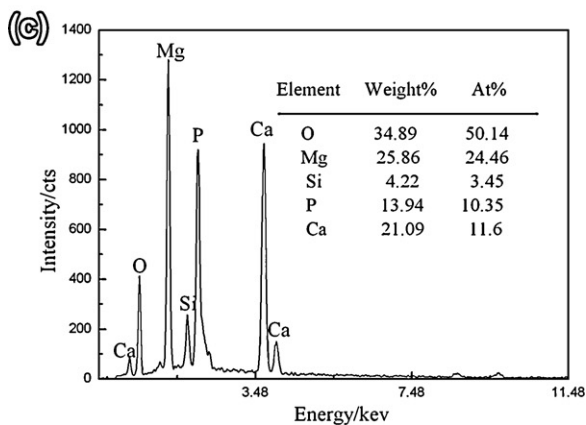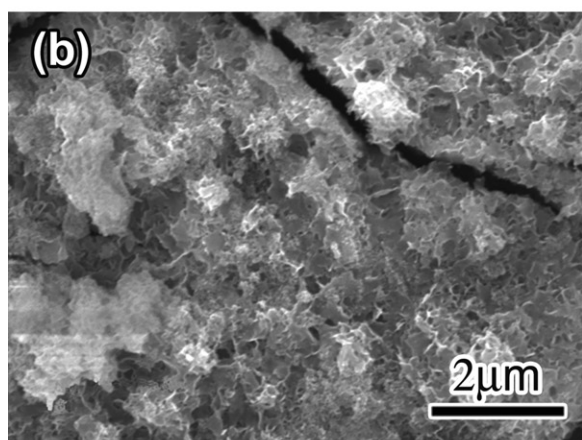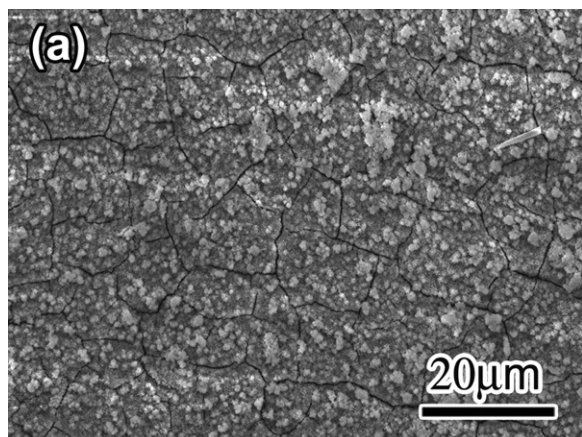
Fig. 1. Surface morphologies of the Mg–Zn–Mn–Ca alloy samples after conversion treatment for 50 min: (a) low magnification, (b) high magnification and (c) EDS of the coating.
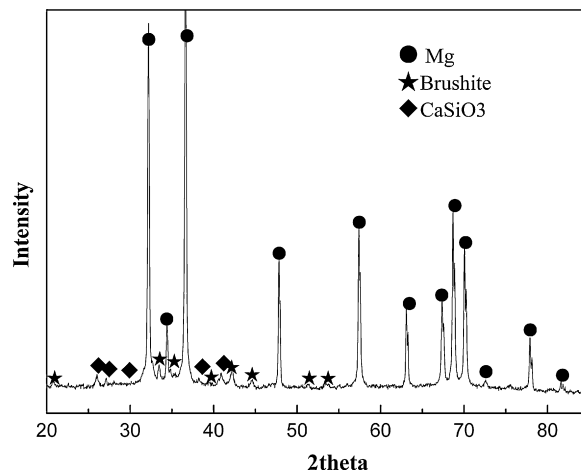

Fig. 2. XRD analysis on the surfaces of Mg alloys after conversion treatment for 50 min.

ple. For example, the corrosion current density decreased by one order of magnitude when it changed from 38.29 μA/cm^2 to 6.1 μA/cm^2, and the corrosion resistance increased from 844 to 3787 Ω/cm^2.

3.3. Cytocompatibility tests

The pH changes in DMEM with the different samples after immersion for 24 h are listed in Table 3. After 24 h immersion, the pH of the DMEM with the bare alloy rapidly increased to 8.00, whereas that of the composite-coated alloy slightly increased,
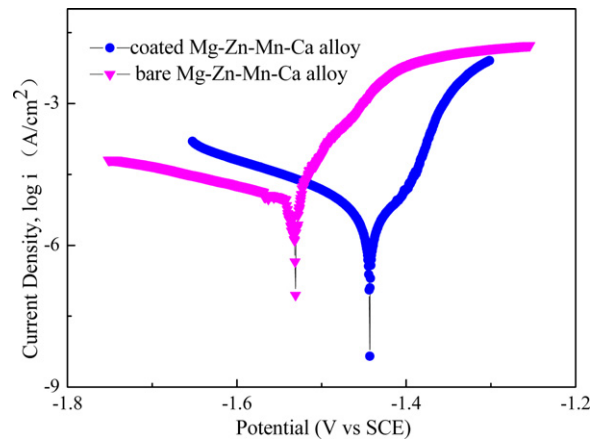
as shown in Fig. 2. The XRD result concludes that the coating is mainly composed of brushite (CaHPO$_4$·2H$_2$O) and small amounts of CaSiO$_3$.

3.2. Electrochemical test

The electrochemical polarization curves of the bare alloy and composite coated alloy are shown in Fig. 3. The corresponding electrochemical data are summarized in Table 2. The most negative corrosion potential (E_{corr}) is obtained for the bare Mg alloy. A significant increase in corrosion resistance (R_p) and a decrease in the corrosion current density (I_{corr}) were observed for the composite coated samples compared with the bare sam-

Fig. 3. The electrochemical polarization curves of the bare Mg–Zn–Mn–Ca alloy and the coated Mg–Zn–Mn–Ca alloy in Hank's solution.

Table 2
Electrochemical parameters of the two samples.

Samples	E_{corr} (mV)	R_p (Ω/cm^2)	I_{corr} (μA/cm^2)
Bare Mg–Zn–Mn–Ca alloy	−1517	844	38.29
Coated Mg–Zn–Mn–Ca alloy	−1432	3787	6.14

Table 3
The pH values of the control DMEM, bare Mg–Zn–Mn–Ca alloy-DMEM and the coated Mg–Zn–Mn–Ca alloy-DMEM after 24 h immersion.

Samples	pH values
Control DMEM	7.40
Bare Mg–Zn–Mn–Ca alloy-DMEM	8.00
Coated Mg–Zn–Mn–Ca alloy-DMEM	7.61

which indicates that the composite coating restrains the corrosion of the alloy.

Cell toxicity test is carried out by evaluating the RGR values of the osteoblasts incubated for 12, 24, 48, and 96 h. Fig. 4 illustrates the RGR values of the osteoblasts on the composite-coated and the bare alloys. A significant increase ($p < 0.05$) in the RGR values is observed in the coated sample extraction medium than that of the bare alloy extraction medium during the whole incubation time, indicating the improved cytocompatibility of the composite coating. According to reference [22] RGR values higher than 75% are considered non-cytotoxic. Therefore, the bare Mg alloy is non-cytotoxic.

The morphologies of the cell adhesions on the bare and composite-coated alloys for different times are presented in Fig. 5. Evident differences were observed in the cells in response to the different surfaces. On the bare alloys, only a few cells are observed on the surface after 6 h incubation, as shown in Fig. 5a. After 12 and 24 h incubation, respectively, limited difference can be found in the cell morphologies and the amount of cells on the bare alloys, as shown in Figs. 5b and c. On the composite-coated samples, some cells with polygonal shape and extended filopodia were observed after 6 h (Fig. 5d). After 12 h incubation, more cells were found on the surface, which were interconnected. After 24 h incubation, the whole surface is covered with a continuous cell layer, as shown in Fig. 5f. By comparison, more cells were observed on the composite-coated alloy than those on the surface of the bare alloy during the whole incubation period, indicating a better cell response to the composite coating. Distinct differences in cell morphology were found on the samples after 24 h incubation under a high magnification, as shown in Fig. 6. The cells on the bare alloy maintained a round morphology (Fig. 6a), whereas the cells connected with each other through thin cytoplasmic digitations and elongation of the cytosols are seen on the composite-coated alloy (Fig. 6b), indicating a good cell response to the composite coating.

Fig. 7 illustrates the cell cycle stage distribution of osteoblasts cultured in the composite-coated DMEM, bare alloy DMEM, and normal DMEM for different periods. The results indicate that the cells in the G_0/G_1 phase did not change significantly at 12 h (Fig. 7a). However, the G_0/G_1 phase in the composite-coated DMEM decreased significantly after 12 h. In addition, a greater percentage of cells in the S phase (Fig. 7b) and the G_2/M phase (Fig. 7c) was observed in the composite-coated DMEM group than those in the normal DMEM and the bare alloy DMEM. These results suggest that the osteoblasts in the composite-coatedalloy DMEM may go

through the cell cycle faster than the control group with a shortened S-G_2 phase.

4. Discussion

Recently, increasing studies have demonstrated that the bioactivity of Ca–P ceramic can be enhanced by incorporating small amounts of physiological ions, such as carbonate [23], Mg [24], and silicate [25]. However, some synthesis methods involving high temperature sintering cannot be used to deposit such a coating on Mg alloy because of its low melting point [26].

In this study, $CaSiO_3/CaHPO_4 \cdot 2H_2O$ composites were coated onto Mg alloys through chemical deposition. H_3PO_4 is hydrolyzed to form H^+ and $H_2PO_4^-$ ions. The $H_2PO_4^-$ reacts with Ca^{2+} to form $Ca(H_2PO_4)_2$. When the Mg alloy is immersed in the reaction bath, the Mg–Zn–Mn–Ca alloy reacts with water to release OH^-. The presence of OH^- facilitates the transformation of $Ca(H_2PO_4)_2$ into $CaHPO_4 \cdot 2H_2O$ [27]. Meanwhile, the Ca^{2+} also reacted with SiO_3^{2-} to form $CaSiO_3$. Eventually, the $CaSiO_3/CaHPO_4 \cdot 2H_2O$ composite coatings are formed on the surface of the Mg–Zn–Mn–Ca alloy. The XRD and EDS results confirmed this as well.

From the electrochemical measurement results, the corrosion rate of the Mg alloy is decreased by the composite coating. In a corrosive environment, the main electrochemical reactions proceed on the exposed surface of the alloy, such that the Mg matrix is dissolved in the anodic areas ($Mg \rightarrow Mg^{2+} + 2e^-$) and the reaction with hydrogen occurs on the cathodic sites ($2H_2O + 2e \rightarrow 2OH^- + H_2\uparrow$). In this study, the $CaSiO_3/CaHPO_4 \cdot 2H_2O$ composites are deposited effectively onto the whole surface of the Mg–Zn–Mn–Ca alloy, impeding the galvanic reaction between the anode and cathode. According to reference [28], the cathodic hydrogen evolution reaction was reduced after an AZ91D substrate was coated with HA; the corrosion potential (E_{corr}) of the HA coating was less than that of the bare AZ91D alloy. In this study, the more negative corrosion potential (E_{corr}) and lower corrosion current density (I_{corr}) are obtained from the composite coating compared with those of the uncoated alloy. Xu et al. [29] suggested that the conversion coating is beneficial for mitigating the corrosion of the Mg alloy substrate. Therefore, the formation of the continuous coating on the whole surface of the alloy can act as a barrier between the alloy and corrosive environment.

The MTT results show that the osteoblast proliferates and survives more quickly in the extraction medium of the composite-coated alloys than those in the extraction medium of the bare alloys after 96-h incubation, indicating that the composite coating has better cytocompatibility. Given that cells are very sensitive to environmental fluctuations, especially changes in pH [30], the fast degradation of the bare Mg alloy results in the high pH in the extraction medium, which has some effects on cell growth. The electrochemical measurements demonstrate that the corrosion rate of the bare alloy is faster than that of the composite-coated alloy. The composite coating controls the degradation rate of the Mg–Zn–Mn–Ca alloy, and prevents sharp pH changes. These provide a suitable bioenvironment for osteoblast proliferation.

The cell adhesion *in vitro* results in this study indicate good cell attachment and proliferation on the composite-coated alloys. Moreover, the composite coating shows greater cell growth compared with the bare alloy. Cell adhesion is sensitive to the morphology of the substrate [31]. The cells show significantly higher levels of attachment on the rough and sandblasted surfaces with irregular morphologies than that on the smooth surfaces [32]. SEM microstructures show that the $CaSiO_3/CaHPO_4 \cdot 2H_2O$ composite has a micro-porous surface structure. In a previ-
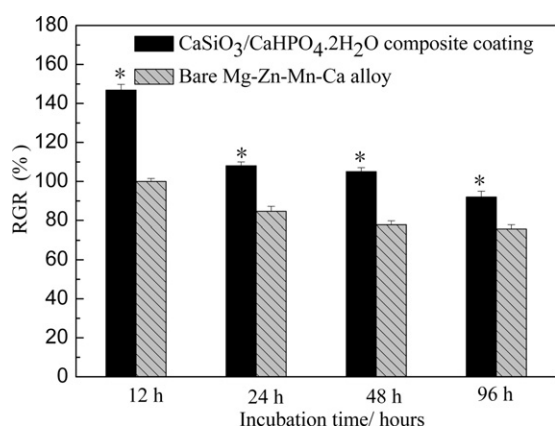

Fig. 4. The relative growth rates of the osteoblast assessed using MTT-based methods at different time points of incubation on the different substrates (*shows signification at $p < 0.05$).
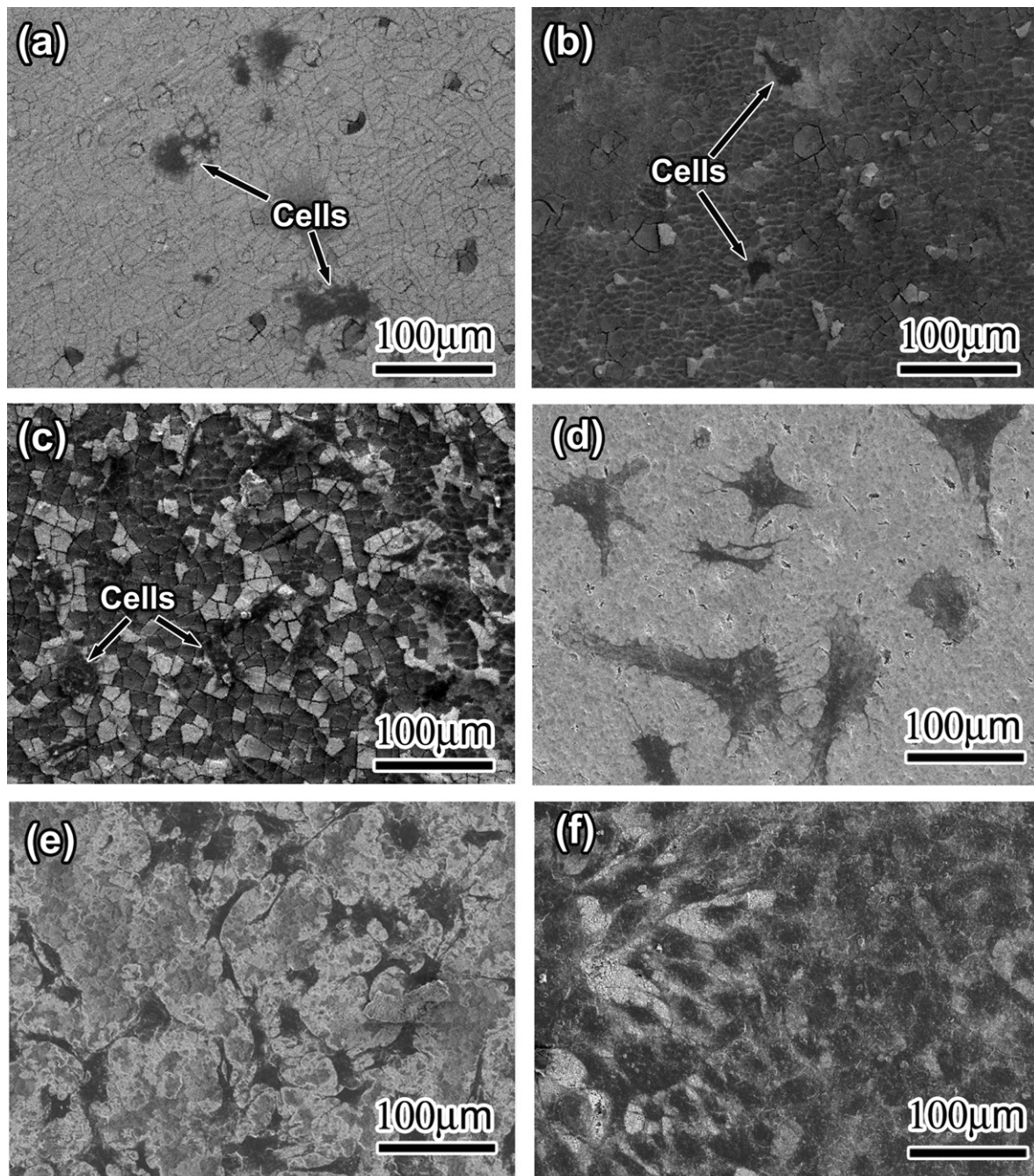
Fig. 5. Cell morphologies at low magnification after the incubation for different times on the samples: (a, b and c) bare Mg–Zn–Mn–Ca alloys for 6, 12 and 24 h, respectively; (d, e and f) CaSiO$_3$/CaHPO$_4$·2H$_2$O composite coated Mg alloys for 6, 12 and 24 h, respectively.

ous paper, the bone regeneration rate on the porous HA and apatite wollastonite glass ceramic is dependent on porosity [33]. The microporous surface structure supposedly enhances cell attachment. Therefore, the surface topographical properties of CaSiO$_3$/CaHPO$_4$·2H$_2$O composite coatings promote osteoblast attachment.

The cellular responses to a material, such as attachment, proliferation, and differentiation, depend not only on the physical properties of the materials, but also on chemical compositions [19]. The composite coating is mainly composed of brushite and CaSiO$_3$. According to a previous study, bone growth on an implant surface requires the presence of sufficient amounts of calcium and phosphate ions [34]. Therefore, CaHPO$_4$·2H$_2$O enhances cellular response. Meanwhile, Si plays a key factor in the coordination control of metabolism and growth in animal cells. Sun et al. [35] has indicated that the ionic dissolution products of dicalcium silicate promote the early proliferation of cells. *In vitro* studies on silicon-substituted hydroxyapatite (Si-HA) by Gibson [36] and the *in vivo* study on Si-HA by Patel [37] suggest that the acceleration of bone apposition for silicon-substituted hydroxyapatite might partly result from an upregulation in osteoblast metabolism. Zhang et al. [38] showed that Si-HA coatings on pure titanium exhibited a higher cell proliferation rate compared with HA coating. In this study, combining the physical characteristics with the chemical composition of the composite coating, we can conclude that the composite coating promotes cell adhesion, which is also confirmed by the cell morphology results.
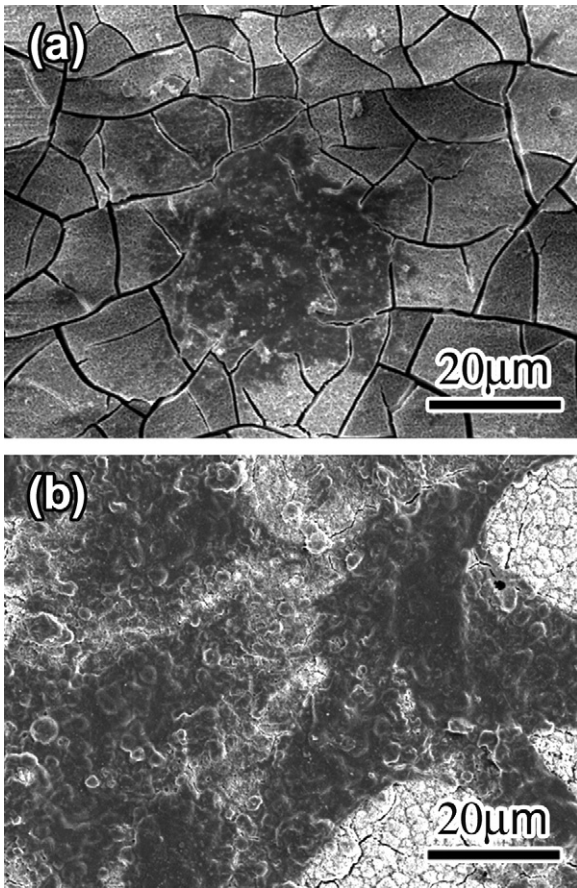
Fig. 6. Cell morphologies at a high magnification after 24 h incubation on different samples: (a) bare Mg–Zn–Mn–Ca alloy; (b) CaSiO$_3$/CaHPO$_4$·2H$_2$O composite coated Mg alloy.
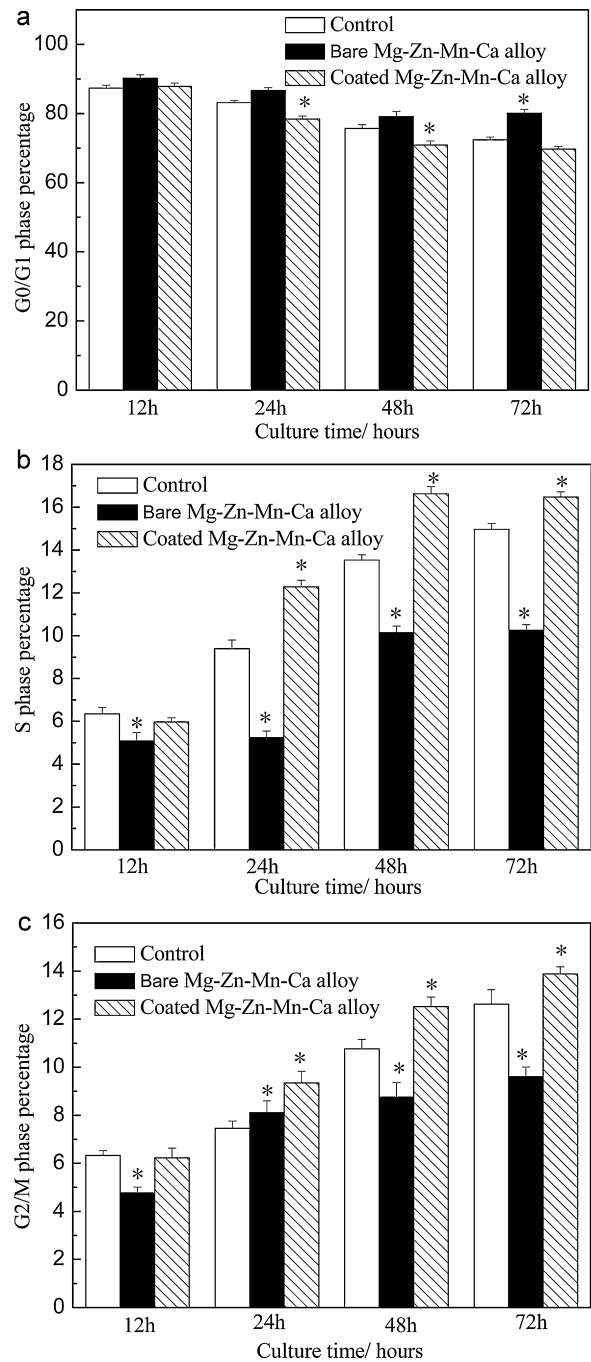

Fig. 7. Cell cycle stage distribution in osteoblast cultured in composite coating-DMEM and normal DMEM: (a) G$_0$/G$_1$ phase percentage; (b) S phase percentage; (c) G$_2$/M phase percentage (*shows signification at $p < 0.05$).

The cell cycle stage *in vitro* results demonstrate that osteoblast proliferation and cell cycle are accelerated by the composite-coated alloys. Theoretically [39], the cell cycle goes from a resting (G$_0$) stage, through the DNA synthetic prophase (G$_1$ phase), a DNA synthetic (S phase), DNA synthetic anaphase (G$_2$ phase), and to the final mitosis (M) stage. Sun [40] has suggested that in some biological systems, the transition from G$_1$ into the S phase is the important stage in the control of cell proliferation. From the results of the cell cycle staging, the composite coating not only increases the transition of the osteoblast from G$_1$ into S phase, but also accelerates that of the osteoblast from S into the G$_2$/M phase. Hence, the composite coating promotes osteoblast proliferation. This is due to the dissolution of the coating surface, which leads to the release of Ca, Si, and P ions. Sun [41] considered the Si ion is a major factor in accelerating the cell cycle and promoting osteoblast proliferation. Keeting [42] proposed that Si stimulates TGF-β1 production in human osteoblasts. Moreover, the existence of Si ion-induced BMP-2 production is believed to stimulate osteoblast differentiation and bone healing [35]. Hattar [43] also suggested that the ion products, especially Si and Ca in this process, might be responsible for the increased cellular expression by Bioglass. Furthermore, CaHPO$_4$·2H$_2$O-coated implants reportedly provide high BMP-2 expression and TGF-β1 expression [12]. Therefore, the ionic products of the composite coating dissolution shortens the osteoblast grow cycle and stimulates osteoblast proliferation. As a surface coating layer, the CaSiO$_3$ and CaHPO$_4$·2H$_2$O composite coating can improve the surface biocompatibility of Mg–Zn–Mn–Ca alloy because the release of the ions from the composite coating plays an active role in osteoblast proliferation.

5. Conclusions

CaSiO$_3$/CaHPO$_4$·2H$_2$O composites were coated onto Mg–Zn–Mn–Ca alloy through a chemical reaction. The CaSiO$_3$/CaHPO$_4$·2H$_2$O composite coatings improved the anti-corrosion resistance of Mg–Zn–Mn–Ca alloy and provided a suitable environment for cell culture. *In vitro* cell tests demonstrated that the composite coatings exhibited a good cellular response due to the presence of CaSiO$_3$ and CaHPO$_4$·2H$_2$O.

Acknowledgement

References

[1] R.C. Zeng, W. Dietzel, F. Witte, N. Hort, C. Blawert, Adv. Eng. Mater. 10 (2008) B3.
[2] C. Di Mario, H. Griths, O. Goktekin, N. Peeters, J. Verbist, M. Bosiers, K. Deloose, B. Heublein, R. Rohde, V. Kasese, C. Ilsley, R. Erbel, J. Interv. Cardiol. 17 (2004) 391.
[3] F. Witte, V. Kaese, H. Haferkamp, E. Switzer, A. Meyer-Lindenberg, C.J. Wirth, Biomaterials 26 (2005) 3557.
[4] F. Witte, J. Fischer, J. Nellesen, H.A. Crostack, V. Kaese, A. Pisch, Biomaterials 27 (2006) 1013.
[5] L. Xu, G. Yu, E. Zhang, F. Pan, K. Yang, J. Biomed. Mater. Res. 83 (2007) 703.
[6] J. Vormann, J. Mol. Asp. Med. 24 (2003) 27.
[7] M.P. Staiger, A.M. Pietak, J. Huadmai, G. Dias, Biomaterials 27 (2006) 1728.
[8] G. Song, Corros. Sci. 49 (2007) 1696.
[9] L.L. Hench, J. Am. Ceram. Soc. 81 (1998) 1705.
[10] K. Cpat, J. Biomed. Mater. Res. 18 (1984) 845.
[11] S. Kotani, Y. Fujita, T. Kitsugi, T. Nakamura, T. Yamamuro, C. Ohtsuki, T. Kokubo, J. Biomed. Mater. Res. 25 (1991) 1303.
[12] L.P. Xu, F. Pan, G.N. Yu, L. Yang, E.L. Zhang, K. Yang, Biomaterials 30 (2009) 1512.
[13] L.T. Arinzeh, T. Tran, J. Mcalary, G. Daculsi, Biomaterials 26 (2005) 3631.
[14] E.M. Carlisle, Science 167 (1970) 279.
[15] K. Schwarz, D.B. Milne, Nature 239 (1972) 333.
[16] W.C. Xue, X.Y. Liu, X.B. Zheng, C.X. Ding, Biomaterials 26 (2005) 3455.
[17] P. Siriphannon, Y. Kameshima, A. Yasumori, K. Okada, S. Hayashi, J. Biomed. Mater. Res. 52 (2000) 30.
[18] P.N. De Aza, Z.B. Luklinska, A. Martinez, M.R. Anseau, F. Guitian, J. Microsc. 197 (2000) 60.
[19] S.Y. Ni, J. Chang, L. Chou, W. Zhai, J. Biomed. Mater. Res. 80 (2007) 174.
[20] S.Y. Ni, K.L. Lin, J. Chang, L. Chou, J. Biomed. Mater. Res. 85 (2008) 72.
[21] ISO-10993-5: Biological Evaluation of Medical Devices – Part 5: Tests for Cytotoxicity: In vitro Methods, China Standard Publication, Beijing, 2000, Attachment 3.
[22] H.P. Hao, The Biological Evaluation Norm and Implementation Guide of Medical Devices, China Standard Publication, Beijing, 2000 (Chapter 7).
[23] E. Boanini, A. Bigi, Thin Solid Films 497 (2006) 53.
[24] S.R. Kim, J.H. Lee, Y.T. Kim, D.H. Riu, S.J. Jung, Y.J. Lee, S.C. Chung, Y.H. Kim, Biomaterials 24 (2003) 1389.
[25] E.S. Thian, J. Huang, S.M. Best, Z.H. Barber, W. Bonfield, Mater. Sci. Eng. C 27 (2007) 251.
[26] H.X. Wang, S.K. Guana, X. Wanga, C.X. Ren, L.G. Wang, Acta Biomater. 6 (2010) 1743.
[27] Y. Wan, G. Xiong, H. Luo, F. He, Y. Huang, X. Zhou, Mater. Design 29 (2008) 2034.
[28] Y.W. Song, D.Y. Shan, E.H. Han, Mater. Lett. 62 (2008) 3276.
[29] L.P. Xu, E.L. Zhang, K. Yang, J. Mater. Sci.: Mater. Med. 20 (2009) 859.
[30] S.X. Zhang, J.N. Li, Y. Song, C.L. Zhao, X.N. Zhang, C.Y. Xie, Y. Zhang, H.N. Tao, Y.H. He, Y. Jiang, Y.J. Bian, Mater. Sci. Eng. C 27 (2009) 1907.
[31] T. Matsuda, J.E. Davies, Biomaterials 8 (1987) 275.
[32] K.T. Bowers, J.C. Keller, B.A. Randolph, D.C. Wick, C.M. Michaels, Int. J. Oral Maxillofac. Implants 7 (1992) 302.
[33] N. Ikeda, K. Kawanabe, T. Nakamura, Biomaterials 20 (1999) 1087.
[34] F. Geng, L.L. Tan, X.X. Jin, J.Y. Yang, K. Yang, J. Mater. Sci.: Mater. Med. 20 (2009) 1149.
[35] J.Y. Sun, L. Wei, X.Y. Liu, J.Y. Li, B. Li, G.C. Wang, F.H. Meng, Acta Biomater. 5 (2009) 1284.
[36] I.R. Gibson, J. Huang, S.M. Best, W. Bonfield, Enhanced in vitro cell activity and surface apatite layer formation on novel silicon-substituted hydroxyapatites, in: O.H. Ohgushi, G.W. Hastings, T. Yoshikawa (Eds.), Proceeding of the 12th International Symposium on Ceramics in Medicine, World Scientific Publishing Co. Singapore, Nara, Japan, 1999, pp. 191–194.
[37] N. Patel, S.M. Best, W. Bonfield, I.R. Gibson, K.A. Hing, E. Damien, P.A. Revell, J. Mater. Med. 13 (2002) 1199.
[38] E.L. Zhang, C.M. Zou, G.N. Yu, Mater. Sci. Eng. C 29 (2009) 298.
[39] C. Norbury, P. Nurse, Annu. Rev. Biochem. 61 (1992) 441.
[40] J.Y. Sun, J.Y. Li, X.Y. Liu, L. Wei, G.C. Wang, F.H. Meng, Biomed. Pharmacother. 63 (2009) 650.
[41] J.Y. Sun, Y.S. Yang, J.P. Zhong, D.C. Greenspan, J. Tissue Eng. Regen. Medk. 1 (2007) 281.
[42] P.E. Keeting, M.J. Oursler, K.E. Wiegand, S.K. Bonde, T.C. Spelsberg, B.L. Riggs, J. Bone. Miner. Res. 7 (1992) 1281.
[43] S. Hattar, A. Asselin, D. Greenspan, M. Oboeuf, A. Berdal, J.M. Sautier, Biomaterials 26 (2004) 839.